4MOST Low Resolution Spectrograph: Design and Performances

F. Laurent, Johan Kosmalski, Didier Boudon, Patrick Caillier, Eric Daguisé, Jean-Emmanuel Migniau, Arlette Pécontal, Johan Richard, Samuel Barden, Olga Bellido-Tirado, et al.

4MOST Low Resolution Spectrograph: Design and Performances

F. Laurent*[a], Johan Kosmalski[a,c], Didier Boudon[a], Patrick Caillier[a], Eric Daguisé[a], Jean-Emmanuel Migniau[a], Arlette Pécontal[a], Johan Richard[a], Samuel C. Barden[b], Olga Bellido-Tirado[b], Steffen Frey[b], Allar Saviauk[b]

[a]Univ Lyon, Univ Lyon1, Ens de Lyon, CNRS, Centre de Recherche Astrophysique de Lyon UMR5574, F-69230, Saint-Genis-Laval, France;

[b]Leibniz-Institut für Astrophysik Potsdam, AIP, An der Sternwarte 16, 14482 Potsdam, Germany;

[c]ESO, Karl-Schwarzschild-Str. 2, D-85748 Garching bei München, Germany;

ABSTRACT

4MOST, the 4m Multi Object Spectroscopic Telescope, is an upcoming optical, fibre-fed, MOS facility for the VISTA telescope at ESO's Paranal Observatory in Chile. Its main science drivers are in the fields of galactic archeology, high-energy physics, galaxy evolution and cosmology. The preliminary design of 4MOST features 2436 fibres split into low-resolution (1624 fibres, 370-950 nm, R > 4000) and high-resolution spectrographs (812 fibres, three arms, ~44-69 nm coverage each, R > 18000) with a fibre positioner and covering an hexagonal field of view of ~4.1 deg². The 4MOST consortium consists of several institutes in Europe and Australia under leadership of the Leibniz-Institut für Astrophysik, Potsdam (AIP). 4MOST is currently in its Preliminary Design Phase with an expected start of science operations in 2021.

Two third of fibres go to two Low Resolution Spectrographs with three channels per spectrograph. Each low resolution spectrograph is composed of 812 scientific and 10 calibration fibres using 85µm core fibres at f/3, a 200mm beam for an off-axis collimator associated to its Schmidt corrector, 3 arms with f/1.73 cameras and standard 6k x 6k 15µm pixel detectors. CRAL has the responsibility of the Low Resolution Spectrographs.

In this paper, the optical design and performances of 4MOST Low Resolution Spectrograph designed by CRAL for 4MOST PDR in June, 2016 will be presented. Special emphasis will be put on the Low Resolution Spectrograph system budget and performance analysis.

Keywords: 4MOST, VISTA, ESO, Spectrograph, Optical Design, Performances

1. INTRODUCTION

4MOST is a wide-field, high-multiplex spectroscopic survey facility under development for the VISTA telescope of the European Southern Observatory (ESO). Its main science drivers are in the fields of galactic archeology, high-energy physics, galaxy evolution and cosmology [1]. 4MOST will in particular provide the spectroscopic complements to the large area surveys coming from space missions like Gaia, eROSITA and Euclid, and from ground-based facilities like VST, DESI, LSST and SKA. The VISTA Wide Field Corrector design provides a focal surface at the conventional Cassegrain focus [2]. 4MOST features a 4.1 degree diameter field-of-view with 2436 fibres in the focal plane that are configured by a fibre positioner based on the tilting spine principle [3]. The fibres feed two types of spectrographs; 1624 fibres go to two spectrographs with low resolution R>4000 and 812 fibres to a high resolution spectrograph with R>18,000 [4]. Both types of spectrographs are fixed-configuration, three-channel spectrographs. 4MOST will have a unique operation concept in which 5 year public surveys from both the consortium and the ESO community will be combined and observed in parallel during each exposure, resulting in more than 25 million spectra of targets spread over a large fraction of the southern sky [5].

*florence.laurent@univ-lyon1.fr; phone +33 4 78 86 85 33; fax +33 4 78 86 83 86; http://cral.univ-lyon1.fr/

This paper will focus on the LRS design which is under CRAL responsibility. The LRS design is driven by providing a high spectral resolution over a large spectral range. Section 2 of this paper introduces the LRS key requirements. Section 3 summarizes the optical design proposed for 4MOST Preliminary Design Review. The key performances coming from the optical design and associated analysis are described in section 4. Finally, section 5, compiles the conclusions and future developments.

2. KEY REQUIREMENTS

The LRS key design requirements are derived from the 4MOST top level requirements ([6] and [7]) and are listed below:

1. The LRS shall be able to accommodate a minimum of 812 science fibres and 10 calibration fibres. It shall accept f/3.0, with 85 micron core diameter fibre inputs. The LRS shall cover simultaneously the wavelength range from 400 nm to 885 nm (goal: from 370 nm to 950 nm). The dichroic transition region shall not include the wavelength ranges 428.3 - 432.1 nm (G-band), 514 – 520 nm (Mgb triplet), and 648 - 666 nm (H-alpha 656.2 nm). The LRS spectra shall be projected on 6k by 6k, 15 micron pixel detector(s).
2. The LRS spectral resolving power shall be:
   - $R \geq 10 \times \lambda/\text{nm}$ for $400\ \text{nm} \leq \lambda < 500\ \text{nm}$, and
   - $R \geq 5000$ for $500\ \text{nm} \leq \lambda \leq 885\ \text{nm}$.

   At any given wavelength, the variation of the LRS spectral resolution shall not exceed 20% PTV over each individual detector.
3. The LRS spectral sampling shall be ≥ 2.5 pixel (goal 3.0 pixels). The variation of the LRS sampling shall be < 50% PTV over each individual detector.
4. The spectrograph shall limit the intensity of any ghost image to less than 0.2% (goal 0.1%) of the intensity of the parent image.
5. At any given wavelength and at all locations of spectra, no spectrum shall contaminate its neighbouring spectra on the detector with more than 2% (goal 1%) of its own flux. The requirement must be fulfilled over 95% (goal 99%) of the detector(s) area.
6. The spectral purity is calculated as a Gaussian fitted to an unresolved emission line which shall contain 85% (goal: 90%) of the fitted line's total flux within ±1 FWHM (2.3 σ) from its centre. The requirement must be fulfilled over 95% (goal 99%) of the detector(s) area.
7. The LRS throughput, defined as the percentage of light available at the exit of the fibre slit surface that is delivered to the detector, shall be greater than 50% at any given wavelength. At any given wavelength, the variation in spectral response shall not exceed 10% (goal: 5%) PTV.
8. The LRS shall be mechanically and thermo-elastically stable to within 1.5 µm over 1 hour.

3. OPTICAL DESIGN

The LRS is composed of 2 identical (or symmetrical) unit spectrographs including the same optical components. Each unitary spectrograph should meet the key requirements listed in section 2. Each spectrograph is fed by an entrance slit of 812 science fibres. After collimation, the optical beam is separated in 3 spectral bandwidths, dispersed and reimaged in 3 different channels with F/1.73 aperture. The separation in three channels provides the minimal resolution of 4000 (Figure 1). The Blue arm goes from 370 to 554 nm, the Green from 524 to 721 and the Red from 691 to 950 nm.
The LRS is composed of the 7 sub-assemblies:

- An entrance slit composed of 812 science fibres following focal plane curvature radius. A Slit Field Lens is glued onto the entrance slit
- A mirror acts as a Collimator collecting the F/3 light from the fibre and generates a collimated beam of 200mm.
- A Dichroic: Dichroic beam splitters in front of the Schmidt corrector separate the three channels. There are two dichroics (Red and Blue).
- In addition, each channel includes a corrector, a VPHG for dispersion, a dioptric camera and a Field Lens Window. The spectral overlap of the channels is determined by the edge of the dichroic and here assumed to be 30nm. A 6k X 6k detector with 15µm/pixel records the spectra.

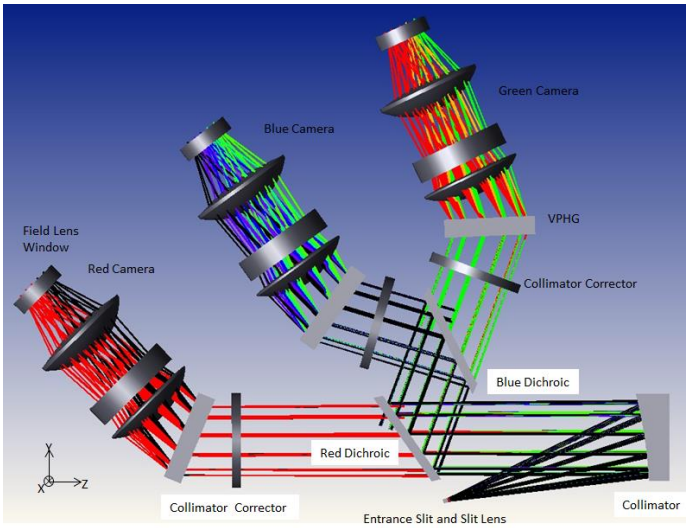

Figure 1: LRS layout

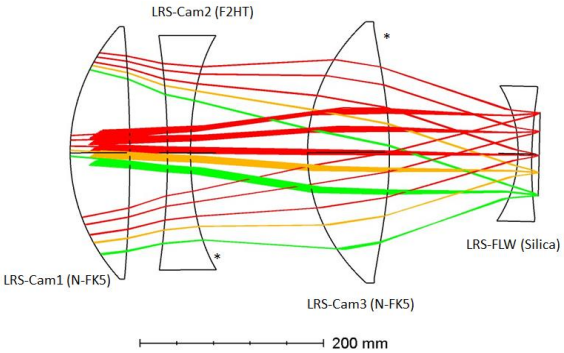

Figure 2: LRS Green Camera Layout

3.1 Entrance Slit and the Slit lens

The entrance slit is composed of 812 science fibres arranged in 28 slitlets of 29 fibres each. Within one slitlet, 2 fibres are separated by 170µm center to center, the slitlets are separated by 5.49mm center to center. 10 optical fibres are located at the edge of the slit for calibration purpose [8]. The fibres follow the focal plane curvature radius of 635mm and are arranged along the Y axis so that the spectra bending by the grating from the center of the slit to the edge is compensated. Thus the spectral lines are flat on the detector.
The slit lens is located at the level of the LRS focal plane so that the Fibre slitlets can be glued onto the first surface of the lens using the appropriate liquid index to reduce Fresnel Losses. The curvature of the first surface of the lens match the Focal Plane curvature and thus all the fibres are virtually gathering in a pupil plane located close to the center of curvature of the Collimator Mirror.

3.2 Collimator, Dichroics and Correctors

The Off-axis Collimator Mirror images the Fibres at infinity and the entrance pupil at the grating level. It collects the F/3 light from the fibre and generates a collimated beam of 200mm. The Off-axis of the Collimator is sufficient to insert the Back Illumination Unit that will act as a shutter and also provided light to measure the position of the Fibres at the Telescope Focal plane.
The separation in wavelength is done by 2 dichroic mirrors reflecting each time the shorter wavelength for a better efficiency. Dichroic beam splitters in front of the Schmidt corrector separate the three channels. There are two dichroics, Red and Blue, tilted by 35 and 43.3 degrees respectively. The wavelength transition regions are 30nm width and are respectively centered at 539nm for the Blue dichroic and at 706nm for Red dichroic.
The Corrector is a plano off-axis asphere corrector. The off-axis matches roughly the off-axis of the collimator mirror. Each corrector is different.
The material of dichroics and correctors are Silica. Their thicknesses are 25mm.

3.3 Grating

Volume-phase holographic gratings (VPHG) have been selected as offering the highest efficiency over a large bandwidth. The three VPHG gratings made of Silica are placed at the average positions of pupil images to optimize their respective sizes of 250mm aperture and feature Bragg angles of 18.35º/22.49º/22.46° with 1351/1220/924 lines/mm (blue/green/red).

3.4 Cameras and Field Lenses

The 3 cameras including 3 lenses work at F/#=1.73 with a focal length of 345mm. All lenses are identical in term of curvature, apertures, thicknesses and asphere coefficients. Only air thicknesses are subject to variation. The bigger lens onto the camera has a 290mm diameter aperture. Moreover, the departure from the best local sphere for the aspheric surfaces does not exceed 1.25mm onto useful aperture compatible with manufacturing constraints. Note that the depth of material that would need to be removed from the best fit sphere is 1.7mm onto diameter. First asphere is on concave surface and second in convex one. A general view of the Green camera can be found in Figure 2. Aspheric surfaces are labeled with (*). Only cheap glasses are used in the camera design (N-FK5 and F2HT).
The Field Lens that makes the enclosure of the detector cryostat is identical for each arm. It is a Silica biconcave lens. The 6k by 6k 15µm pixel detector is at 4mm from the back surface of the lens.
Each camera has a different decenter along the spectral direction and tilt with respect to the grating. Each Field Lens is centred with respect to its CCD. Each detector assembly has a different focus position, a decentering along the spectral direction and tilt with respect to the camera to compensate for axial color.

4. PERFORMANCES

The following sub-section presents the performance of the current design based on a geometric optics and system assessments for 4MOST PDR in June, 2016. They correspond to on-going work for FDR with possible improvements.

4.1 Assumptions

The LRS analysis takes into account these following assumptions:

- In order to show the performances along the slit, 5 representative fields along +x-axis and 5 wavelengths are selected per arm.
- The raw data come from various Zemax PSFs which are oversampled (0.256µm per zemax pixel). The convolution between Zemax PSFs and mock fibre is rebinned onto LRS detector pixels (ie. 15µm per pixel).
- Detector characteristics are defined with flatness irregularity, charge diffusion and pixelisation. The LRS design shall consider a detector flatness irregularity of ± 20 µm PTV. The FWHM of a Gaussian fit to the detector charge diffusion curve is in the order of 0.86px @450nm, 0.75px @600nm, 0.5px @800nm. The detector uses 15µm pixel.
- The scattered light is simulated according to the VPHG model derived from HERMES spectrograph data [9]. The difference here is that the convolution kernel is a 2D one, assuming the scattered light will occur in both spatial and spectral direction. This is a kind of worst case study.

4.2 Global Parameters

The LRS accommodates a minimum of 812 science fibres and 10 calibration fibres. It shall accept f/3.0 fibre inputs with 85 micron core diameter fibre inputs. The LRS covers simultaneously the wavelength range from 370 nm to 950 nm. The dichroic transition region excludes wavelengths from the G-band, Mgb triplet and H-alpha. The LRS spectra are projected on 5957 x 6074 pixels², 15 micron pixel detector giving margins for MAIV.

4.3 Spot Diagram

The image quality of the LRS is directly related to the spectral sampling and spectral resolving power requirements. No requirements onto Gaussian FWHM PSF or RMS Spot Radius or Ensquared Energy are given. Unfortunately, these last data are often used when an optical layout is designed. To reach 4000 in spectral resolving power, the average maximal spectral sampling in FWHM is 3.1 pixels. That is equivalent to Gaussian FWHM PSF of 23µm, RMS Spot radius of 13.9µm and 95% of Ensquared Energy in 38.5µm². The total budget in image quality is shared in 5 parts (design/manufacturing/assembling/environment/margin), the quadratic sum of which should stay within the main system budget. For the LRS optical design, an average RMS Spot Radius requirement of 11µm with a goal at 10µm is acceptable. In average, the LRS RMS spot radius is well below 10µm with a maximum value of 20µm for few point of the FoV and for extreme wavelength (Figure 3and Figure 4).

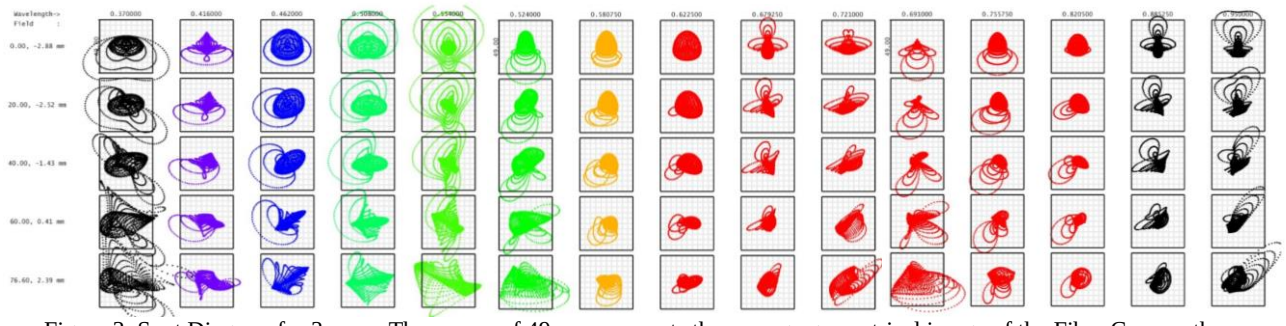

Figure 3: Spot Diagram for 3 arms; The square of 49µm represents the average geometrical image of the Fibre Core on the detector

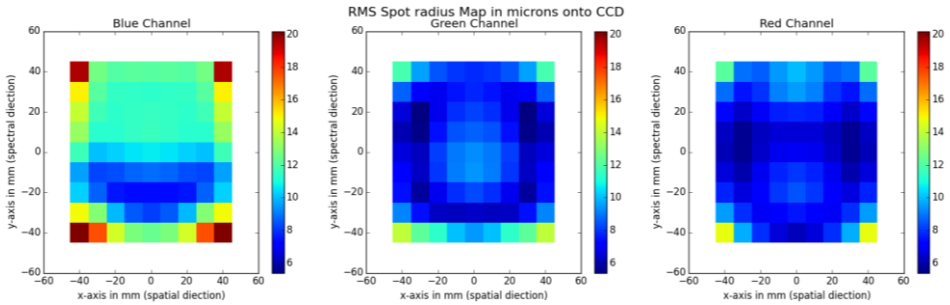

Figure 4: RMS Spot radius distribution onto CCD for the 3 channels

4.4 Spectral Resolving Power

The delta_lambda is defined as the width of a resolution element. It is given by the full width at half-maximum (FWHM) of a fit (Gaussian or better) in spectral direction to an unresolved, well-exposed, spatially collapsed emission line. Moreover, spectral sampling is defined as the size in pixels of delta_lambda, i.e. the width of a resolution element.

The spectral resolving power is computed using the following method. The pixellated image is collapsed into a one-dimensional line spread function in the spectral direction by summing rows of five pixels centred on the geometric image (Figure 5). A Gaussian fit (or better) is made to the line spread function, and the full-width-half-maximum of the fitted curve is obtained. This FWHM defines the resolving element of the spectrograph.

The FWHM derived from a Gaussian fit is very optimistic, as it increases the obtained resolution by a factor 1.35 with respect to the 1D profile of the fibre at its center. The actual fibre-convolved image does not resemble a Gaussian fit and therefore we propose a more realistic, custom model to estimate the spectral resolution. In this custom model, the Line Spread Function is modelized using a filled circle, mimicking the fibre convolved by a PSF modelled as a circular 2D Gaussian (parametrised by its FWHM). This convolved circle is rebinned (resampled) using the detector pixel size and summed up over 5 pixels in the spatial direction. The best model is found by minimizing the difference between this model and the raw data (also summed over 5 pixels in spatial direction) using a least squares algorithm. Currently the raw data are provided by the optical PSF derived from Zemax, convolved by a mock fibre (as for the model), rebinned onto detector pixels and summed up over 5 pixels (Figure 5). We tested this custom model with simulated raw data using various Zemax PSFs and fibre locations, and find it more realistic than the simple Gaussian fit, giving a spectral resolution increased by a factor 1.18.

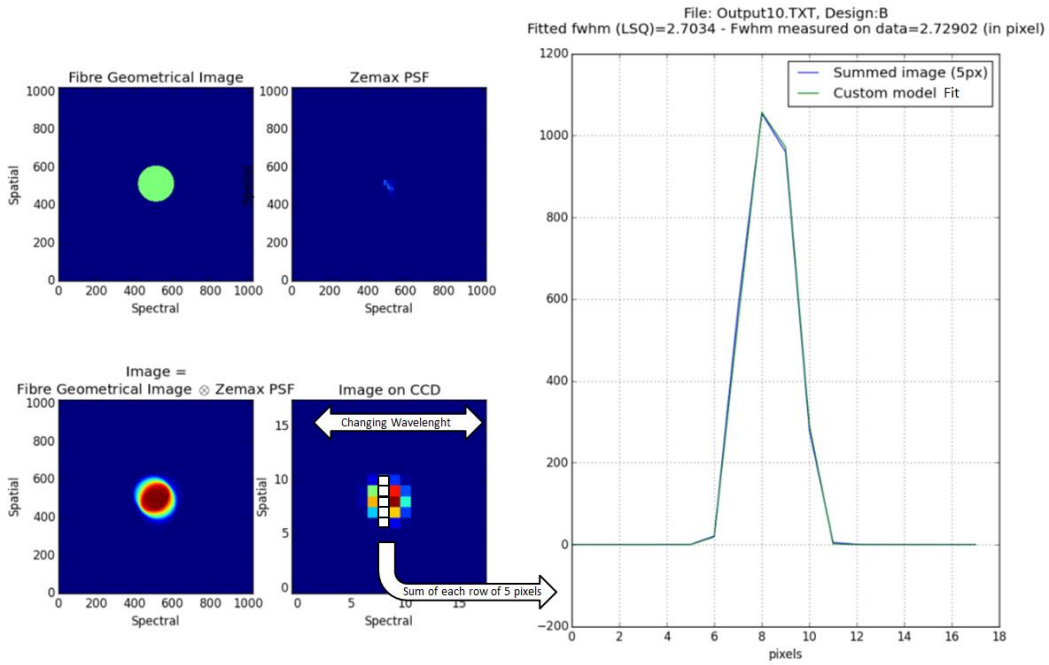

Figure 5: Custom model. (Left) simulated raw fibre image: the circular fibre (upper-left panel) is convolved by the theoretical PSF from Zemax (upper-right panel), then projected onto the CCD pixel grid (bottom right panel). (Right) the summed image over the central 5 detector columns (blue curve) is fit by the custom model (green curve)

Including optical design itself, CCD flatness, detector charge diffusion, scattered light and thermal effect, the spectral resolving power is still compliant with requirements and gives margins for MAIV phase (Figure 6). Note that is the worst case.

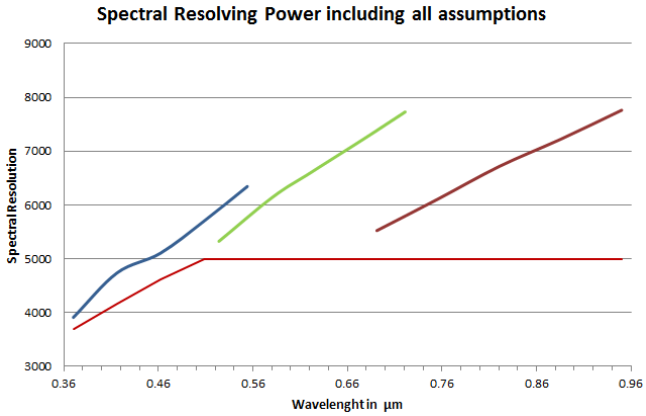

Figure 6: Spectral resolution including optical design, CCD flatness, Detector Charge Diffusion, thermal effect and scattered light

4.5 Spectral Sampling

The spectral sampling calculation is derived from spectral resolving power calculation method (§ 4.3). Including optical design itself, CCD flatness, Detector Charge Diffusion, scattered light and thermal effect, the spectral sampling is still compliant with requirements with a median value of 2.92 pixels (Figure 7). Note that is the worst case.

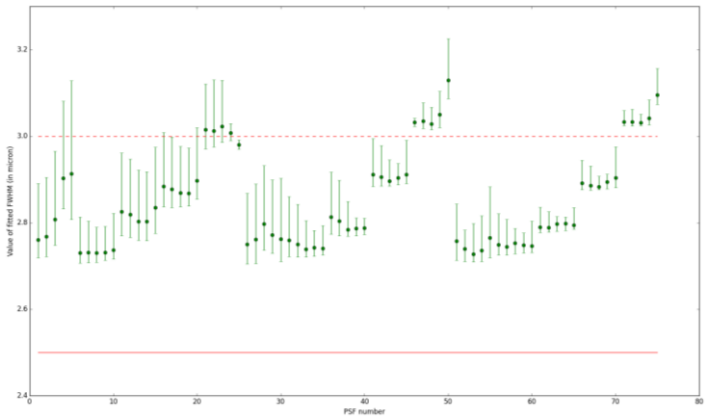

Figure 7: Spectral sampling including optical design itself, CCD flatness, Detector Charge Diffusion and scattered light

4.6 Ghosts Analysis

The ghost image analysis is performed with Zemax. The optical transmission or reflection of the element is based on a conservative approach and the preliminary coating design. The assumption takes into account as following:

- Detector reflectance is 10% average
- Collimator mirror is protected silver with a reflectance of 98%
- AR coating efficiency of 99%
- Dichroic Efficiency of 95% reflectance at shortwave, 95% transmittance at longwave for dichroic coating, 2% AR coating at longwave for the other surface.
- VPHG efficiency of 80% in transmission in order 1 and 16% in transmission in order 0.
- VPHG recombination efficiency of 1% in reflection for order 0 and 1.

In the LRS optical system, there are six lenses, one collimator mirror, 2 dichroics, one VPHG and one detector. The total number of optical surfaces to be considered in the ghost image analysis is 17. The potential ghost images would be more hundred cases. However, it is not necessary to analyze all the ghost images. The screening technique is used based on the ghost image size and flux. The fluxes' ratio between the ghost image and the parent image is calculated on an area of 1 CCD pixel. This study was performed only onto blue arm which should be the more sensitive.
Ghost images given by 2nd order pollution, back face of the dichroic, camera lenses, corrector, slit and field lenses have a ratio well below 10^{-5}.

The optical ghosts are generated when using VPHG in spectrographs employing the Littrow configuration [10]. The ghost is caused by white light reflected off the detector surface, recollimated by the camera, recombined by, and reflected from, the grating and reimaged by the camera onto the detector. This recombination can occur in two different ways:

- “Reflective” ghost: That is a dispersive (i.e., non-specular) reflection off of the grating back toward the camera
- “Transmissive” ghost: That is dispersive transmission through the grating, then reflection off of the air-glass interface of the grating substrate on the far side, followed by a zeroth order transmission back through the grating, sending the light in the direction of the camera.

Taking into account assumptions defined before, the Littrow ghost intensity has a ratio below 1.6e-3 with respect to any real image for the primary ghost onto an area representing 9% of the detector area. For the secondary one, the ratio is 3.5e-6. The Figure 8 presents a zoom view of the Littrow ghost in yellow. The red vertical line is the flat continuum for one single fibre (ie. the real spectra), the green vertical blur is the reflection of the Littrow ghost dispersed again by the grating.

The Littrow ghost is at the limit of the requirements but it strongly depends on assumptions which are pessimistic.

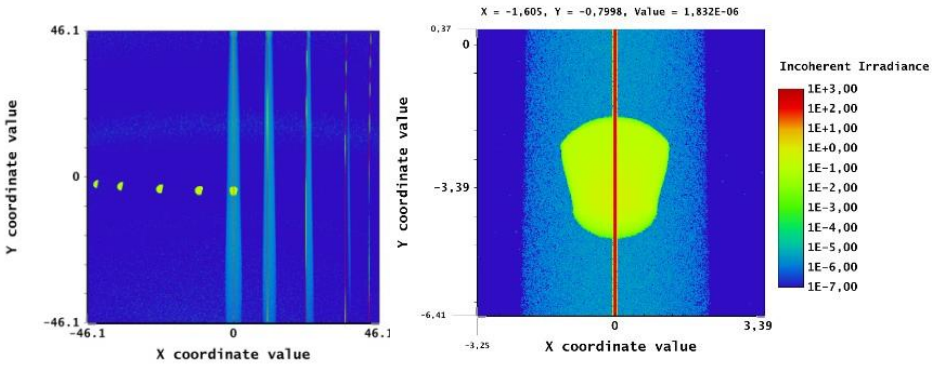

Figure 8: Non-Sequential Mode. Left: Littrow Ghost for 5 fibres. Right: Zoom view of the Littrow Ghost

4.7 Crosstalk

The crosstalk criterion is derived by computing the ratio between the flux contained in a box centered on the LSF (3x3 box width) and the same box separated by 6.5 pixels on the spatial direction. Taking into account optical design itself, CCD flatness, Detector Charge Diffusion, scattered light and thermal effect, the crosstalk is ~ 0.72%, compliant with requirements. The main contribution comes from the scattered light.

4.8 Spectral Purity

The purity criterion is defined as a ratio of the integral of the custom model fitted on the LSF curve summed over 5 pixels restricted to the window [-FWHM:+FWHM] around the center over the total flux of the LSF curve summed over 5pixels. The fwhm value has been measured on the custom model curve. Taking into account optical design itself, CCD flatness, Detector Charge Diffusion, scattered light and thermal effect, the spectral purity is above 85% within requirements (Figure 9).

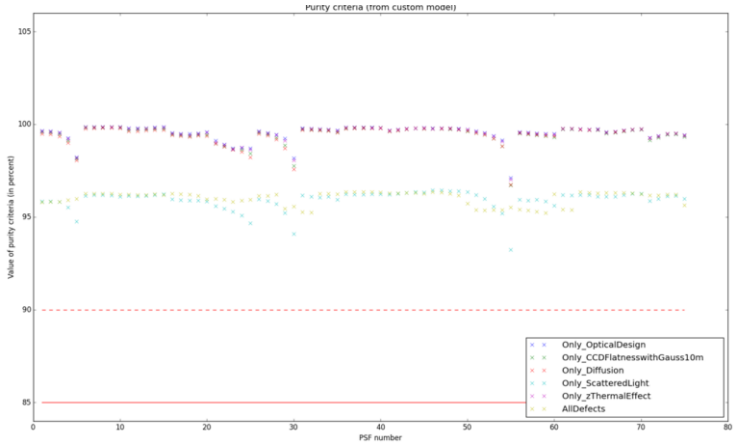

Figure 9: Spectral Purity between spectra for optical design, charge diffusion and scattered light and all computed with Custom model fit.

4.9 Throughput

The LRS throughput estimation takes into account the internal glass transmission, the dichroics, the coating of collimator mirror, the VPHG efficiency and the antireflective coatings. The CCD is not included in this budget.

For dichroics, the transmission / reflectivity specification is estimated to 98% / 97%. A silver coating reflectivity at 98% has been taken as a theoretical average for the collimator mirror reflectivity. To reach the spectral resolution, the optical beam is passing through 11 AR coated surfaces excluding the VPHG and dichroic. A specified value at 99% is required. The use of VPHG providing good transmission over large spectral domains renders making the LRS an efficient

spectrograph possible. Nevertheless, significant effect of the VPHG on the edges of the domains strongly affects the minimum throughput values. There is the same effect for dichroics in their transition bands.

Figure 10 illustrates the corresponding throughput assessment at PDR phase, 62.7% in average for 50.3% in minimum is achieved over the whole contractual bandwidth (400-885nm). In blue wavelength and in dichroic transitions, the throughput is out of specification of 10% due to VPHG and dichroics. To enhance the throughput, given the number of pieces to be AR coated, special care shall be taken on the specification which could be to 99.5%.

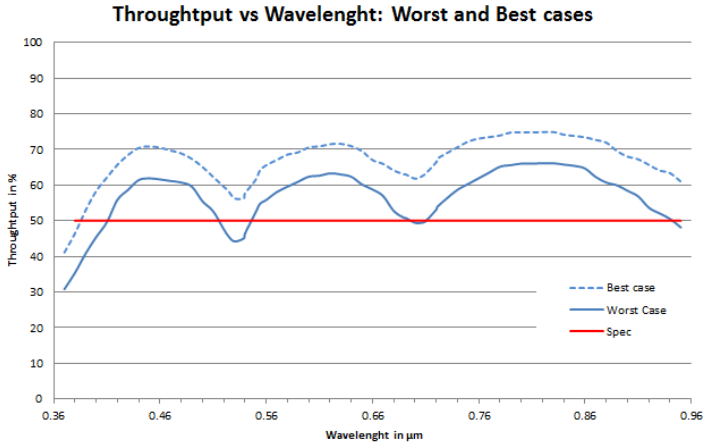

Figure 10: LRS throughput estimation with supplier data

4.10 Spectral Stability

For this analysis, the thermal performance of the LRS over a 0°C to 20°C temperature range is analyzed. Morevover, the Paranal pressure varies between 700 mbar and 800 mbar with an average of 750 mbar. Using Zemax only effects along the optical axis can be simulated, a Finite Element Analysis (FEA) of the LRS opto-mechanical design will be provided at a later stage of the project. For the analysis, a whole bench in aluminum (CTE 24.10-6 /°C) is considered. It takes into account variations on refractive index, lenses radii and thicknesses. With 1°C variation, the spectra are shifted of 2.0µm in X spatial direction and 1.8µm in Y spectral one. Moreover, the defocus value due to temperature variation is +1.1µm/°C if an invar Camera/Detector interface is used. Otherwise, variation is +4.82µm/°C. Due to Paranal air pressure change (±50mbar), the average best focus change is ±11 µm.

Using different pupil profiles given by 3 different fibre tilts (0.0°, 1.9°, 2.7°) - Figure 11 and [8], the position of the field onto CCD is evaluated. The maximal deviation is 0.8µm for 1.9° tilt and 1.6µm for 2.7° tilt (Figure 12). The LRS thermal damping or control is still under investigation. With this thermal damping or control, the LRS focus will stay at the best position and within requirements.

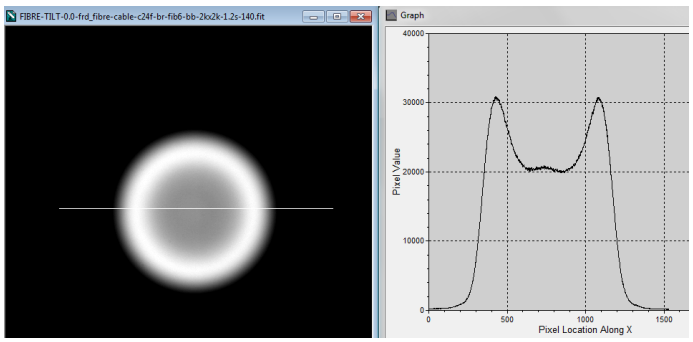

Figure 11: A sample of far field images of the 80µm core fibres

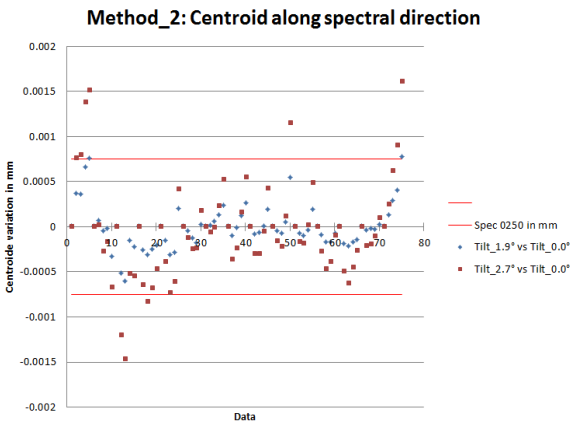

Figure 12: Position of the centroid along spectral direction when fibre has different tilts

4.11 Sensitivity and Tolerance Analysis

The alignment sensitivity analysis was done using Zemax. The approach to the analysis was as follows:

- Beginning with the nominal LRS optical design, each optical group was individually perturbed a prescribed amount in each degree of freedom (DOF). For most groups, the perturbations that were modeled were lateral displacement (x, y), angular rotation (θx, θy, θz), and longitudinal displacement (z).
- The sensitivity analysis is performed onto 12 optical groups (Slit, Entrance Slit, Slit Field Lens, Collimator, Dichroic Red and Blue, Corrector, VPHG, Camera (composed of 3 lenses), Field Lens Window (FLW), CCD and Detector Vessel - DV(composed of Field Lens Window and CCD).
- Two changes in the system were evaluated onto the CCD plane at central wavelength for each arm:
    - The image shift along x and y-axes (shift of 4 FoV corresponding to the 4 CCD corners are averaged),
    - The RMS spot radius (RSCE) degradation (Average of 9 FoV onto 5 wavelengths that means 45 data).
- Dividing the change in the RSCE by the magnitude of the perturbation yields the Alignment Sensitivity for that optic in that DOF.
- The Alignment Sensitivity for each optic was then multiplied by the alignment tolerance assigned to that optic for that DOF.
- A table was then created, listing the Alignment Sensitivities of each optic, and their prescribed tolerances in each DOF (Table 1). The results were summed in rms, and the total is entered into the LRS system Budget.

The main contributors for the image shift are the Collimator (θx, θy), the Dichroics (θx, θy), the Camera [(θx, θy) or (x, y)], the DV (x, y) and CCD (x, y).
The main contributors for the spot radius degradation are the Camera (z), DV (z), CCD (z) and the Collimator (θx, θy).

First, the tolerancing analysis is performed onto blue arm without compensator. The Table 1 gives the tolerances to reach image quality and image shift requirements. The nominal tolerances (±0.5mm / ±5arcmin) are relevant. The introduction of compensators is mandatory due to tight tolerances done by tolerance analysis without compensator.
Second, to reach image quality and image shift requirements, the following adjustments are set: the entrance slit as reference, the Collimator in (x, y), the Dichroics in (θx, θy), the VPHG in (θz), the Camera in (x, y) and the DV in (x, θx, θy). All other degrees of freedom are set at the nominal positioning (±0.5mm / ±5arcmin).

Table 1: Tolerances to reach image quality and image shift requirements (in red the more stringent tolerances)

	X (µm)	Y (µm)	Z(µm)	Tx (arcsec)	Ty (arcsec)	Tz (arcsec)
Slit	63	63	51	299	173	150
Slit Field lens	500	500	500	299	299	299
{Slit+Slit Field lens}	63	63	50	60	166	75
Coll Mirror	63	63	50	9	9	75
Dichro_Red	500	500	258	9	9	299
Dichro_Blue	500	500	250	9	9	299
Corrector	500	262	500	299	299	299
VPGH	500	500	500	299	299	19
Camera+DV	500	500	500	19	19	150
Camera	31	31	16	37	37	299
DV	31	31	16	78	79	150
FLW	128	98	66	229	299	299
CCD	31	31	16	118	152	150

4.12 Impact of the Slitlet Arrangement

Due to the manufacturing process of each individual slitlet and then their assembly, the theoretical position and orientation of each individual fibres cannot be rigorously achieved.
First, the slitlet will be polished flat. Thus all 29 fibres within one slitlet will have the same chief ray angle. This creates an oversizing of the pupil of ~4.5mm (2.1%) along the spatial axis (for a nominal diameter of 200mm). This has a negligible impact on the image quality. Second, the flat surface of the slitlet prevents from a perfect optical contact with the Slit Lens. A gap from 11µm to 15µm along the optical axis for the slitlet at the center of the FoV up to 20 to 24µm at the edge of the FoV is obtained. As this gap will be filled with an index matching gel, the defocused introduced is then negligible. Third, the mount for the slitlets assembly will be done using a 5-axis CNC machine. The Theta X of the individual slitlet cannot be performed. The impact in pupil and image quality is more visible for the outermost slitlets. This creates an oversizing of the pupil of ~5mm (2.5%) along the spectral axis (for a nominal diameter of 200mm). This has a negligible impact on the image quality.

Now, all LRS optical components are oversized enough so that there is no vignetting but if we implement a pupil stop with the exact 200mm diameter, a vignetting up to 2.5% is expected in both directions. This has a negligible impact on the image quality.

5. CONCLUSION AND FUTURE DEVELOPMENT

Since Optical PDR, a big effort from CRAL has been made to pay attention onto Optical PDR non-compliances which were mass, volume, ghosts and throughput. CRAL team has managed to propose an affordable LRS opto-mechanical design. This new LRS optical design satisfies most of scientific requirements including throughput, ghosts, new wavelength range and spectral resolving power. Nevertheless, the analysis presented here shows that the design of 4MOST LRS is compliant, except for one requirement with its technical specifications. The partial compliance is the Spectrograph stability. LRS thermal damping or control is still under investigation. With this thermal damping or control, the LRS focus will stay at the best position. For the Final Design Review, CRAL team will pay attention onto this partially compliance.

In conclusion, the LRS optical design still provides margins in the critical areas of image quality and spectral resolving power. There is then a good hope that the finally build LRS spectrographs will match its ambitious scientific performances.

REFERENCES

[1] Roelof de Jong et al., "4MOST: the 4-metre Multi-Object Spectroscopic Telescope project at preliminary design review," Proc SPIE 9908, 61 (2016)

[2] Nicolas Azais et al., " Wide-field corrector for 4MOST: design details and MAIV processes," Proc SPIE 9908, 308 (2016)

[3] Andrew I. Sheinis et al., "The Australian ESO positioner (AESOP) for 4MOST facility on the Vista Telescope," Proc SPIE 9908, 306 (2016)

[4] Walter Seifert et al., "4MOST: the high-resolution spectrograph," Proc SPIE 9908, 335 (2016)

[5] Jakob C. Walcher et al., " 4MOST: science operations for a large spectroscopic survey program with multiple science cases executed in parallel," Proc SPIE 9910, 69 (2016)

[6] Steffen Frey et al., "4MOST preliminary instrument design," Proc SPIE 9908, 310 (2016)

[7] Olga Bellido-Tirado et al., " 4MOST systems engineering: from conceptual design to preliminary design review," Proc SPIE 9911, 76 (2016)

[8] Dionne M. Haynes et al., "4MOST fibre feed preliminary design: prototype testing and performance," Proc SPIE 9908, 317 (2016)

[9] G. Raskin et al., “HERMES: a high-resolution fibre-fed spectrograph for the Mercator telescope,” A&A 526, A69 (2011)

[10] Burgh et al., “Recombination Ghosts in Littrow Configuration: Implications for Spectrographs Using Volume Phase Holographic Gratings,” PASP 119, 859 (2007)